Hindawi
Advances in Mathematical Physics
Volume 2024, Article ID 4519487, 16 pages
https://doi.org/10.1155/2024/4519487

*Research Article*

# Approximate Analytical Solution of the Influences of Magnetic Field and Chemical Reaction on Unsteady Convective Heat and Mass Transfer of Air, Water, and Electrolyte Fluids Subject to Newtonian Heating in a Porous Medium

**M. Sulemana**,[1] **Y. I. Seini**,[1] **and O. D. Makinde**[2]

[1]*Department of Mathematics, Faculty of Physical Sciences, University for Development Studies, Nyankpala Campus P.O. Box, 1350, Tamale, Ghana*
[2]*Faculty of Military Science, Stellenbosch University, Private Bag X2, Saldanha 7395, South Africa*

Correspondence should be addressed to M. Sulemana; musahsulemana@uds.edu.gh

Received 24 April 2023; Revised 1 November 2023; Accepted 21 December 2023; Published 30 January 2024

Academic Editor: Luigi C. Berselli



This paper addresses the unsteady hydrodynamic convective heat and mass transfer of three fluids namely air, water, and electrolyte solution past an impulsively started vertical surface with Newtonian heating in a porous medium under the influences of magnetic field and chemical reaction. Suitable dimensionless parameters are used to transform the flow equations and the approximate analytic method employed to solve the flow problem. The results are illustrated graphically for the velocity, temperature, and concentration profiles. Though, low Prandtl numbers produce high-thermal boundary layer thickness, however, as a novelty, the presence of the magnetic field delayed the convection motion hence, the thermal boundary layer thickness is greater for water with high $P_r = 7.0$ as compared to air with low $P_r = 0.71$ and electrolyte solution with low $P_r = 1.0$. Practically, water with a high-Prandtl number can effectively absorb and release heat. This makes water useful in applications such as geothermal heat pumps and solar thermal collectors, industrial processes such as chemical reactions, distillation, and drying, and in oceanography in predicting the movement and behavior of ocean currents, which in turn can impact weather patterns and climate. Another major observation from the study is that the rate of cooling associated with air, water, or electrolyte impacts differently on the product being cooled.

## 1. Introduction

Free convection or natural convection is a self-sustained flow that takes place as a result of buoyant force due to difference in densities caused by the difference in temperature. In natural convection, the flow is not influenced by any external source like a fan, pump, suction device, etc. Examples of free convection flow include boiling water, hot air rising, cooling of hot objects, thermosiphon cooling, geothermal vents, ocean currents, forest fires, etc. Three fluids are used in this study namely air, water, and electrolyte solution due to their importance in life. For instance, air is very important for the survival of most living things on earth as it provides oxygen necessary for respiration. It also plays an important role in the planet's climate and weather systems as well as in the ozone layer that protects the earth from harmful ultraviolent radiation from sun. Water is a universal solvent that dissolves a wide range of substances, making it crucial component in many chemical reactions in living organisms. Water is also a good conductor of heat and electricity, making it essential for regulating body temperature and transmitting nerve impulses. An electrolyte solution is a liquid that contains dissolved ions that can conduct electricity. Electrolyte solutions are important in many biological and chemical processes, including transmission of nerve impulses in the body, functioning of batteries, production of metals through electrolysis, etc. In the current study, an attempt is made to consider the influence of radiation, magnetic field, and chemical reaction on the free convection flow with Newtonian heating in porous medium as discussed in the details below.

Time-dependent free convection heat and mass transfer has a wide range of of industrial applications. As a result of this, many researches have focused their attention on unsteady free convective heat and mass transfer, which the current study also seeks to contribute. Heat and mass transfer occur in several processes such as wire drawing, hot rolling, fiber drawing, continuous casting, drying, evaporation of water at surfaces, etc. In practice, industrial processes depend on time; and this unsteadiness in the flow is caused by either the impulsive motion of the external stream or the time-dependent motion of the external stream. Siegel [1] was among the early researchers who studied time-dependent free convection flow under step-change in wall temperature through a semi-infinite vertical plate using the momentum integral method. It was observed that the temperature and velocity fields exhibited the same behavior. Martynenko et al. [2] built upon Siegel's work by subjecting the plate and the surrounding stationary fluid to a constant temperature.

Radiation plays a useful role in free convective flow or in heat transfer especially at high temperatures in industrial systems such as rocket propulsion systems, aerothermodynamics, plasma physics, etc. Therefore, many researchers into convection flows have included radiation effects in the flows for industrial purposes. Das et al. [3] used Laplace transform to study convection flow through impulsively started vertical plate subject to the radiation effects. Again, Das et al. [4] built on the work of Das et al. [3] to add partial slip to the flow. Manjunatha et al. [5] studied the effect of radiation on fluid flow and heat transfer over an unsteady stretching sheet and observed that radiation has great impact in the rate of heat transfer in the boundary layer region. Das et al. [6] studied unsteady convection flow with thermal radiation using Laplace transform and observed that the increase in radiation parameter is higher in uniform heat flux than in the uniform wall temperature. Das and Jana [7] also used Laplace transform technique to investigate natural convective flow with radiation heat transfer and noticed that as the radiation parameter increased, the velocity as well as the temperature of the fluid decreased in the region of the boundary layer. Similarly, Mohamed et al. [8] used Runge–Kutta–Fehlberg (RKF) to analyze the effect of thermal radiation on fluid flow in a permeable plate with Newtonian heating and noticed the wall temperature increased due to the presence of radiation parameter. Basant and Gabriel [9] examined the effect of radiation on fluid flow on a flat plate using RKF fourth–fifth order techniques and noticed that the radiation parameter increased the thermal boundary layer thickness. Hussain et al. [10] studied nonsimilar modeling of electromagnetic radiative flow using finite-difference method and concluded as one of their major findings that limiting convection across boundaries reduced the entropy generation.

Many researchers have also worked on the area of magnetohydrodynamics (MHD) in porous medium. Therefore, MHD free convective flow in porous medium has significant engineering applications. For instance, magnetic field effects in the industrial and engineering systems are very essential in the functionality of these systems. It is useful in chemical engineering to investigate filtration process where magnetic filters remove iron particles from the products that are liquid or slurry form; in agricultural engineering to investigate underground water; in petroleum engineering to investigate the movement of oil or gas. As a result of the industrial applications of MHD flow in porous medium, many researchers studied MHD flow in a porous medium with distinct flow configurations, which the present study also seeks to contribute. Hsiao [11, 12] studied MHD convection flow using finite-difference method and MHD stagnation flow with viscous dissipation effect. He observed in both studies that the strength of the magnetic field affects the rate of heat transfer. Similarly, Nadeem et al. [13] used the Runge–Kutta method to investigate MHD fluid properties embedded in porous medium and concluded that the flow is retarded by the presence of the magnetic field. Seini and Makinde [14] studied MHD flow on stretching surface with chemical reaction and radiation and observed that radiation parameter and the magnetic field decreased the rate of heat transfer. Ali et al. [15] considered boundary flow through an inclined stretching sheet with the magnetic field. The temperature equation contained a nonlinear velocity term with MHD just as in the study of Seini and Makinde [14], Sulemana and Seini [16], and Sulemana et al. [17]. It was observed that increased in magnetic parameter, Eckert number, or Prandtl number decreased the velocity profile while increased in Grashof number increased the velocity profile. Das and Jana [7] studied magneto-convective flow and observed that presence of the magnetic field and radiation parameter enhanced temperature as well as the velocity of the fluid. Ahmed et al. [18] applied numerical/analytical solutions for MHD flow embedded in porous medium over oscillating vertical sheet and observed that increased in either the radiation parameter or the permeability parameter decreased the velocity and the temperature profiles. Ibrahim and Tulu [19] used spectral quasilinearization method (SQLM) to solve MHD boundary layer flow on a wedge with heat and mass tranter in porous medium and concluded that an increased in either the magnetic or the permeability parameters reduced the velocity boundary layer thickness. Jabeen et al. [20] analyzed MHD flow in porous medium subject to suction and injection using semi-analytical method and observed that the flow field is effectively appreciable by suction and injection. The effects of radiation, thermal slips, and velocity in MHD heat and mass transport in porous medium were studied by Reddy et al. [21] using Keller-Box technique. They found out that temperature of the fluid dropped due to the improvement in the heat factor and the slip parameter. Similarly, to the work of Reddy et al. [21], a magnetohydrodynamic flow in a porous medium was analyzed by Arul Vijayalakshmi et al. [22] using the homotopy perturbation technique and observed that the fluid thickened, thermal boundary layer thickness decreased due to increment in the radiation parameter. Hussain et al. [23] studied the impact of nonsimilar modeling of mixed convective flows of nanofluids past vertical permeable surface applying local nonsimilarity technique via bvp4c and observed a reversed flow for the velocity profile due to variation in the nonsimilar variable.

Also, the influence of chemical reaction in convective flows in many engineering systems or industrial processes cannot be overlooked. An investigation into the flow over an unsteady stretching surface with chemical reaction subject to the heat source was studied by Seini [24]. He observed that an increased in the unsteadiness parameter increased mass and heat transfer rates and the skin friction coefficient. Sulemana et al. [25] also used Laplace transform techniques to study unsteady MHD flow on a vertical surface with chemical reaction. Similarly, Sulemana and Seini [16] studied time-dependent hydromagnetic flow across a porous vertical surface with internal heat generation in the presence of chemical reaction. In both studies, they concluded that as time passed, skin friction coefficient reduced. Krishna et al. [26] applied Laplace transform method to study unsteady MHD flow in porous medium and observed that increase in permeability parameter increased the fluid velocity and shear stress. Recently, Sulemana et al. [17] studied MHD hydrodynamic boundary layer flow in an unsteady porous medium using approximate analytical method and concluded that chemical reaction parameter as well as permeability of porous medium are effective in reducing skin friction and are importance in practice since reduced skin friction enhances a system efficiency.

It must be noted that thermal boundary conditions of a free convective flow determine the characteristics of heat transfer. Therefore, in Newtonian heating, the heat transfer rate from the boundary surface with finite heat capacity is proportional to the local surface temperature and this process is called conjugate convective flow. Many engineering devices such as fins, heat exchangers, and solar radiation devices are designed based on this configuration. Hence, it is important to consider convective flows subject to the Newtonian heating. Chaudhary and Jain [27] employed Laplace transform techniques to investigate unsteady free convection flow in an impulsively started vertical plate with Newtonian heating and noticed that the temperature distribution decreased as Prandtl number increased. Narahari and Nayan [28] extended the work of Chaudhary and Jain [27] using Laplace transform method to obtain exact solution of an impulsively started free convection flow in vertical plate subject to Newtonian heating with mass diffusion and thermal radiation and observed that aiding flows increased the velocity while opposing flows decreased the velocity of the fluid. Das et al. [4] reported the effects of radiation on free convection unsteady flow through a vertical plate subject to the Newtonian heating using implicit finite-difference method of Crank–Nicolson's type. It was realized that the velocity near the plate decreased while the velocity away the plate increased. Hussanan et al. [29] used Laplace transform techniques to analyze unsteady flow and heat transfer of a Casson fluid through an oscillating vertical surface subject to Newtonian heating and concluded that an increased in Casson parameter increased the velocity while an increase in Newtonian heating parameter increased the thermal boundary thickness. Sharidan et al. [30] employed Laplace transform method to study the slip effects on unsteady convective heat and mass transfer subject to Newtonian heating and observed that slip parameter presence reduces the fluid velocity. An investigation of the effects of Soret on unsteady MHD mixed convective flow in a porous medium with Newtonian heating was also done by Hussanan et al. [31] using Laplace transform techniques. They noticed that increasing values of Soret number increased the fluid concentration and velocity. Konwar et al. [32] built on Hussanan et al. [31] work's to consider an MHD heat and mass transfer of a Newtonian fluid mixture on an exponentially stretched sheet in porous medium with temperature-dependent fluid properties, Soret and Dufour effects. They observed that flow, heat, and mass transfer are significantly influenced by mixed convection parameters, magnetic field, permeability, conductivity, Prandtl number, viscosity and Schmidt number.

In the literature, it is clear that most of the studies focused on the radiation effects on convection flows as well as flows of the different configurations. The main aim of this paper is therefore to investigate the influences of magnetic field and chemical reaction on unsteady hydrodynamic convection heat and mass transfer of air, water, and electrolyte fluids subject to Newtonian heating in porous medium, just as in [33] but solved with new enhanced technique. The present study is an extension of the work of Chaudhary and Jain [27] to include the influences of magnetic field and chemical reaction in the flow under unsteady conditions. The authors introduced a novel approach called approximate analytic method (AAM), to investigate the present study and established that in the absence of magnetic field [27, 28] low-Prandtl numbers produce high-thermal boundary layer thickness, however, in the presence of the magnetic field (present study) the thermal boundary layer thickness is greater for water with high $P_r = 7.0$ as compared to air with low $P_r = 0.71$ and electrolyte solution with low $P_r = 1.0$.

## 2. Problem Formulation

Motivated by hydromagnetic applications in engineering, in this study, incompressible, optically dense viscous unsteady hydromagnetic convective mass, and heat transfer flow past infinite impulsively started vertical surface subject to Newtonian heating is considered. Three (3) fluids: water, air, and electrolyte solution are used in this study. From Figure 1, the $x^* -$ axis which is along the plate is chosen as the flow direction and normal to the plate is the $y^* -$ axis. For time $t^* \leq 0$, i.e., at rest, the fluid exhibits a constant temperature of $T^*_\infty$ while the plate has a constant concentration of $C^*_\infty$. For time $t^* > 0$, the plate experienced an impulsive motion in vertically upward direction with a uniform velocity $v$, temperature $T^*_w$ and the concentration $C^*_w$. Figure 1 shows the flow system.

The plate is infinitely along the $x^* -$ direction, hence all the physical variables are the functions of $y^*$ and $t^*$ only. Under Boussinesq approximation, neglecting the inertia terms, Soret effects, viscous dissipation, and Dufour effects, the equations governing the flow, similar to the study by Chaudhary and Jain [27, 28] are:

$$\frac{\partial u^*}{\partial x^*} + \frac{\partial v^*}{dy^*} = 0, \tag{1}$$

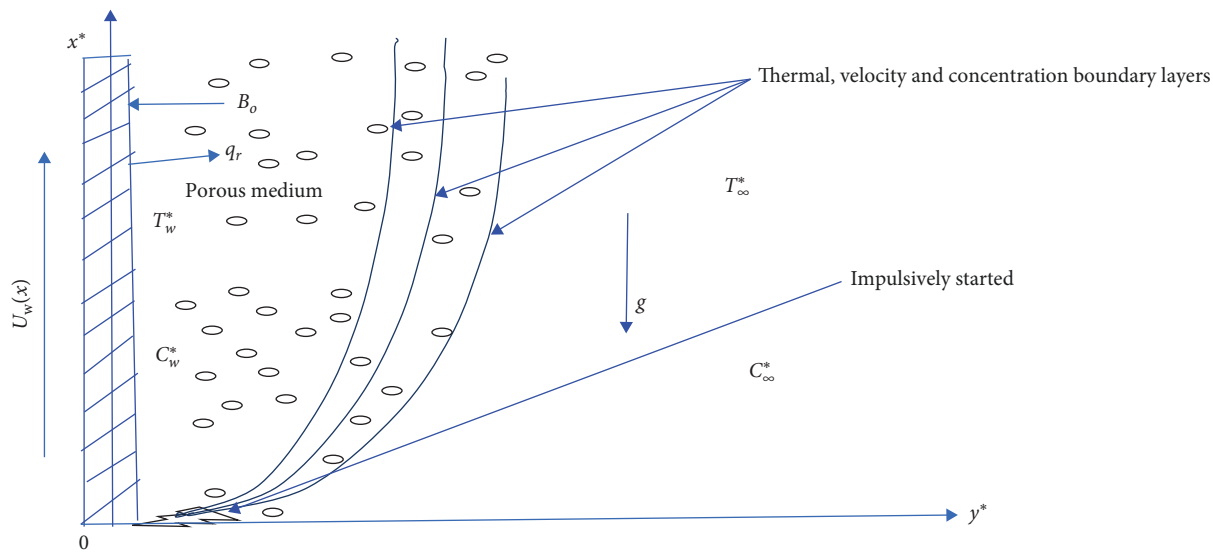


FIGURE 1: The fluid flow system.

$$\frac{\partial u*}{\partial t*} - \mathrm{v}\frac{\partial u*}{\partial y*} = \nu\frac{\partial^2 u*}{\partial y*^2} + g\beta_T(T* - T_\infty*) + g\beta_C(C* - C*_\infty) - \frac{\sigma B_0{}^2}{\rho}u^*, \tag{2}$$

$$\frac{\partial T^*}{\partial t^*} - \mathrm{v}\frac{\partial T^*}{dy^*} = \alpha\frac{\partial^2 T^*}{\partial y^{*2}} - \frac{1}{\rho c_p}\frac{\partial q_r}{\partial y^*} + \frac{\sigma B_0^2}{\rho c_p}, \tag{3}$$

$$\frac{\partial C*}{\partial t*} - \mathrm{v}\frac{\partial C^*}{dy^*} = D\frac{\partial^2 C*}{\partial y*^2} - K_C(C* - C*_\infty), \tag{4}$$

with boundary conditions similar to the study by Chaudhary and Jain [27, 28]:

$$u^* = 0, \mathrm{v}^* = 0, T^* = T_\infty^*, C^* = C_\infty^* \text{ for all } \mathrm{y}^* \geq 0, \mathrm{t}^* \leq 0, \tag{5}$$

$$u^* = U_0,\ T^* = T_w^*, C^* = C_w^* \text{ at } \mathrm{y}^* = 0, \mathrm{t}^* > 0, \tag{6}$$

$$u^* \to u_\infty^*, T^* \to T_\infty^*, C^* \to C_\infty^* \text{ as } \mathrm{y}^* \to \infty, \mathrm{t}^* > 0. \tag{7}$$

Introducing dimensionless parameters similar to Narahari and Nayan [28], Sharidan et al. [30], and Chaudhary and Jain [27] as follows:

$$u = \frac{u^*}{\mathrm{v}},\ y = \frac{y^*\mathrm{v}}{\upsilon},\ \theta = \frac{T^* - T_\infty^*}{T_w^* - T_\infty^*},\ E_c = \frac{u^2}{C_p(T_w^* - T_\infty^*)},\ t = \frac{t^*\mathrm{v}^2}{\upsilon}, \tag{8}$$

$$c = \frac{C^* - C_\infty^*}{C_w^* - C_\infty^*},\ P_r = \frac{\upsilon}{\alpha},\ G_r = \frac{\upsilon g\beta_T(T_w^* - T_\infty^*)}{\mathrm{v}^3},\ G_c = \frac{\upsilon g\beta_C(C_w^* - C_\infty^*)}{\mathrm{v}^3}, \tag{9}$$

$$k_c = \frac{\nu k_c^*}{U_0^2},\ F = \frac{16\sigma a^*\upsilon^2 T_\infty^{*3}}{k^* U_0{}^2},\ S_c = \frac{\nu}{D},\ M = \frac{\sigma B_0^2\upsilon}{\rho\mathrm{v}^2},\ Da = \frac{\mathrm{v}^2 k^*}{\upsilon^2}. \tag{10}$$

Using the Rosseland approximation

$$\frac{\partial q_r}{\partial y^*} = -4a^*\sigma(T_\infty^{*4} - T^{*4}). \tag{11}$$

Assuming that the temperature differences with the flow are sufficiently small such that $T^{*4}$ is expressed as a linear function of the temperature. By Taylor series expansion neglecting the higher order terms, $T^{*4}$ is expressed as a linear function of the temperature in the form:

$$T^{*4} \approx 4T_\infty^{*3}T^* - 3T_\infty^{*4}. \tag{12}$$

Substituting Equation (12) into Equation (11):

$$\frac{\partial q_r}{\partial y^*} = -4a^*\sigma(T_\infty^{*4} - 4T_\infty^{*3}T^* + 3T_\infty^{*4}), \tag{13}$$

$$= -4a^*\sigma(4T_\infty^{*4} - 4T_\infty^{*3}T^*), \tag{14}$$

$$= -16a^*\sigma(T_\infty^{*4} - T_\infty^{*3}T^*), \tag{15}$$

$$\frac{\partial q_r}{\partial y^*} = -16a^*\sigma T_\infty^{*3}(T_\infty^* - T^*). \tag{16}$$

Substituting Equation (16) in Equation (3) and the transformation of Equation (10) in Equations (1)–(4) give the following dimensionless models:

$$\frac{\partial u}{\partial t} - \frac{\partial u}{\partial y} = \frac{\partial^2 u}{\partial y^2} + G_r\theta + G_c c - Mu, \tag{17}$$

$$\frac{\partial \theta}{\partial t} - \frac{\partial \theta}{\partial y} = \frac{1}{P_r}\left(\frac{\partial^2 \theta}{\partial y^2} - F\theta\right) + ME_c u^2, \tag{18}$$

$$\frac{\partial c}{\partial t} - \frac{\partial c}{\partial y} = \frac{1}{S_C}\frac{\partial^2 c}{\partial y^2} - k_C c. \tag{19}$$

Subject to the boundary conditions in dimensionless form:

$$u = 0,\ \theta = 0,\ c = 0,\ \text{for all } y \geq 0,\ t \leq 0, \tag{20}$$

$$u = 1,\ \theta = 1, c = 1,\ \text{for all } y = 0,\ t > 0, \tag{21}$$

$$u \to \infty, \theta \to \infty, c \to \infty \text{ as y} \to \infty, \text{t} > 0. \tag{22}$$

## 3. Approximate Analytic Method

AAM is used to solve the nonlinear dimensionless Equations (17)–(19) with boundary conditions in Equation (22). These nonlinear equations can be integrated numerically, however in this study since the Reynolds number is small, approximate analytic solution can be obtained by some perturbation on the nonlinear equations. Therefore, a linear approximated solution of the nonlinear equations can be obtained by applying the approximate analytic method.

Consider the concentration model in Equation (19), using power series to expand in terms of Eckert number gives:

$$\sum_{i=1}^{n} c_n'(t)E_c^n(y) - \sum_{i=1}^{n} c_n(t)\frac{\partial}{\partial y}E_c^n(y) = \frac{1}{S_c}\sum_{i=1}^{n} c_n(t)\frac{\partial^2}{\partial y^2}E_c^n(y) - k_c\sum_{i=1}^{n} c_n(t)E_c^n(y). \tag{23}$$

The coefficients terms $c_0 > c_1 > c_2\ldots$ in power series, therefore higher terms are negligible. Also, in this study, the Eckert number ($E_c$) such that $E_c < 1$, therefore higher terms $E_c^2 E_c^3$, $E_c^4$, …, are negligible.

Now, considering powers of $E_c$;

$$E_c^0 : c_0' - c_1\frac{\partial E_c}{\partial y} = \frac{2c_2}{S_c}\left(\frac{\partial E_c}{\partial y}\right)^2 + \frac{c_1}{S_c}\frac{\partial^2 E_c}{\partial y^2} - k_c c_0, \tag{24}$$

$$E_c^1 : c_1' - 2c_2\frac{\partial E_c}{\partial y} = \frac{6c_3}{S_c}\left(\frac{\partial E_c}{\partial y}\right)^2 + \frac{2c_2}{S_c}\frac{\partial^2 E_c}{\partial y^2} - k_c c_1, \tag{25}$$

$$E_c^2 : c_2' - 3c_3\frac{\partial E_c}{\partial y} = \frac{3c_3}{S_c}\frac{\partial^2 E_c}{\partial y^2} - k_c c_2. \tag{26}$$

In Equation (26) and considering appropriate boundary conditions in Equation (22) for the concentration profile gives:

$$c_2(t) = e^{-k_c t}. \tag{27}$$

Applying Laplace transform to Equations (24) and (25) gives:

$$s\bar{c}_1(y,s) - c(y,0) - \frac{2}{s+k_c}\frac{\partial \overline{E}_c}{\partial y} - \frac{2}{S_c}\frac{1}{s+k_c}\frac{\partial^2 \overline{E}_c}{\partial y^2} + k_c\bar{c}_1(y,s) = 0, \tag{28}$$

$s$ is the Laplace transform parameter.

Considering appropriate boundary conditions in Equation (22) for the concentration profiles Equations (24) and (28) and using convolution theorem, the general solution of the concentration model is:

$$c(y,t) = c_o + c_1 E_c + c_2 E_c^2 + \ldots, \tag{29}$$

$$c(y,t) = e^{-2S_c y} + e^{-S_c(y-1)}E_c + e^{-k_c t}E_c^2. \tag{30}$$

Similarly, by considering the dimensionless temperature model in Equation (18) and the dimensionless velocity model in Equation (17), expanding in power series in terms of Eckert number, the general solutions are, respectively;

$$\theta(y,t) = e^{-P_r y} + e^{-P_r y}E_c + e^{-\frac{F}{P_r}t}E_c^2, \tag{31}$$

$$u(y,t) = e^{-y} - e^{-2y-Mt}(G_r\theta_1(y,t) + G_c c_1(y,t))\left[\frac{e^{Mt}}{M} - \frac{1}{M}\right]E_c + \left[e^{-Mt} + \frac{1}{M}(G_r\theta_2(y,t) + G_c c_2(y,t))\right]E_c^2, \tag{32}$$

where

$$c_1(y,t) = e^{-S_c(y-1)}, \tag{33}$$

$$c_2(y,t) = e^{-k_c t}, \tag{34}$$

$$\theta_1(y,t) = e^{-P_r y}, \tag{35}$$

$$\theta_2(y,t) = e^{-\frac{F}{P_r}t}. \tag{36}$$

*3.1. Other Possible Solutions for the Velocity Model.* Since, the ratio of momentum diffusivity to thermal diffusivity of the fluid is characterized by the Prandtl number, $P_r = 1$ represents fluids whose thermal boundary layer thickness and momentum have the same order of magnitude. For all values of $P_r$ except $P_r = 0$, the temperature as well as the velocity

solutions in Equations (31) and (32), respectively, are valid. It must be noted that $P_r = 0$ is not possible in practice and therefore has no effect in the solution obtained.

Case 1: When $\boldsymbol{k_c = 1}$ and $\boldsymbol{P_r = 1}$.

$$u(y,t) = e^{-y} - e^{-2y-Mt}\left(G_r e^{-y} + G_c e^{-S_c(y-1)}\right)\left[\frac{e^{Mt}}{M} - \frac{1}{M}\right]E_c + \left[e^{-Mt} + \frac{1}{M}\left(G_r e^{-Ft} + G_c e^{-t}\right)\right]E_c^2. \tag{37}$$

Case 2: When $\boldsymbol{k_c \neq 1}$ **and** $\boldsymbol{P_r = 1}$.

$$u(y,t) = e^{-y} - e^{-2y-Mt}\left(G_r e^{-y} + G_c e^{-S_c(y-1)}\right)\left[\frac{e^{Mt}}{M} - \frac{1}{M}\right]E_c + \left[e^{-Mt} + \frac{1}{M}\left(G_r e^{-Ft} + G_c e^{-k_c t}\right)\right]E_c^2. \tag{38}$$

*3.2. The Rate of Heat Transfer Coefficient of the Unsteady Hydromagnetic Flow.* On the stretched plate, the heat transfer coefficient rate can be investigated in terms of Nusselt number, $Nu$. The $P_r$ and $E_c$ effects on $Nu$ can be investigated. The dimensionless Nusselt number is:

$$N_u = -\frac{\partial\theta}{\partial y}_{|y=0} = P_r(1 + E_c). \tag{39}$$

*3.3. The Rate of Mass Transfer Coefficient of the Unsteady Hydromagnetic Flow.* At the stretching plate, the mass transfer coefficient rate can be determined in terms of Sherwood number, $Sh$. The $E_c$ and $S_c$ effects on Sherwood number are investigated. The Sherwood number is as follows:

$$sh = -\frac{\partial c}{\partial y}_{|y=0} = S_c(2 + e^{Sc}E_c). \tag{40}$$

*3.4. The Skin Friction Coefficient of the Unsteady Hydromagnetic Flow.* The variations in skin friction due to the physical parameters $t, M, E_c, S_c, P_r, G_r$, and $G_c$ can be investigated. The skin friction is as follows:

$$\tau = \frac{\partial u}{\partial y}_{|y=0} = 1 - \left[2e^{-Mt}\left(G_r + G_c e^{S_c}\right) - e^{-Mt}\left(-G_r P_r - G_c S_c e^{S_c}\right)\right]\left[\frac{e^{Mt}}{M} - \frac{1}{M}\right]. \tag{41}$$

## 4. Results and Discussion

Numeric values of the temperature, concentration, and velocity fields are computed and shown in the figures to measure the effects of the physical parameters such as $t, P_r, S_c, G_r, G_C, M, F, E_c$, and $K_c$ on the hydromagnetic flow. Water, air, and electrolyte solution are used in the study.

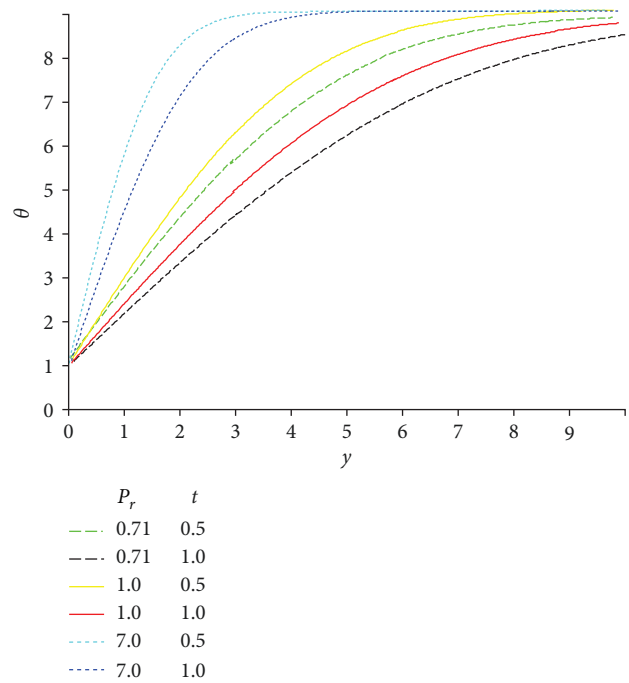


Figure 2: (Present study with magnetic field presence). Temperature profile for water ($P_r = 7.0$), air ($P_r = 0.71$), and electrolyte solution ($P_r = 1.0$) and when $E_c = 0.9$ and $F = 2$.

The values of the Prandtl number, $P_r$ are taken as 7.0 for water, 0.71 for air, and 1.0 for electrolyte solution and the values of the Schmidt number $S_c$ are taken as 0.62 for water, 0.24 for air, and 0.67 for electrolyte solution. These are physical values of $S_c$ and $P_r$ of these fluids.

### 4.1. Graphical Results

*4.1.1. Temperature Profiles.* In Figure 2, the effects of the Prandtl number on the temperature profile for water with $P_r = 7.0$, air with $P_r = 0.71$ and electrolyte solution with $P_r = 1.0$ are considered. Low-Prandtl numbers produce high-thermal boundary layer thickness [27, 28], however, in Figure 2, it is observed that the presence of the magnetic field delayed the convection motion. Also, the molecules of water are closer to each other than air, they get charged up faster than air in the presence of magnetic field hence a reversed flow occurred. Hence, the thermal boundary layer thickness is greater for water with high $P_r = 7.0$ as compared to air with low $P_r = 0.71$ and electrolyte solution with low $P_r = 1.0$. Practically, water with a high-Prandtl number can effectively absorb and release heat. This makes water useful in applications such as geothermal heat pumps and solar thermal collectors and in oceanography in predicting the movement and behavior of the ocean currents, which in turn can impact weather patterns and climate.

Figures 3–5 show the effects of Eckert number $E_c$ on the temperature profile for water $P_r = 7.0$, electrolyte solution $P_r = 1.0$, and air $P_r = 0.71$, respectively. It is noticed that temperature falls for the positive values of $E_c$ while for the negative values of $E_c$ the reverse occurred as the time passes. In general, an increase in the Eckert number leads to an increase

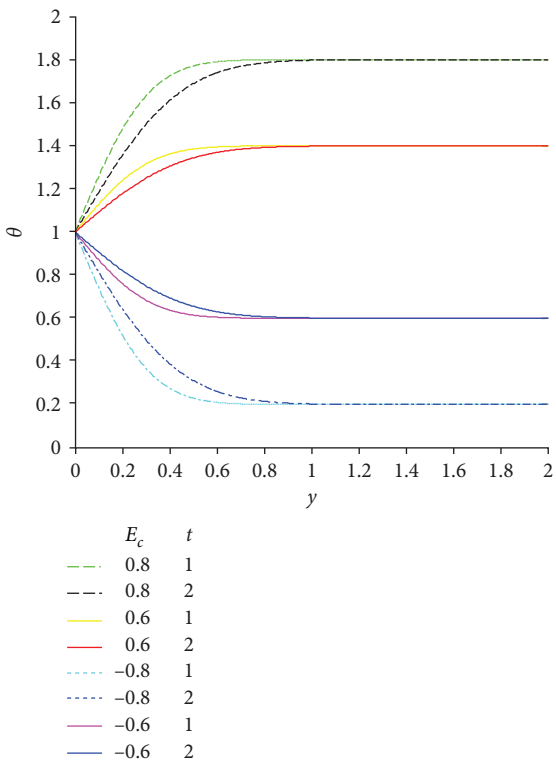


FIGURE 3: Temperature profile of the effect of $E_c$ on water ($P_r = 7.0$) when $F = 2$.

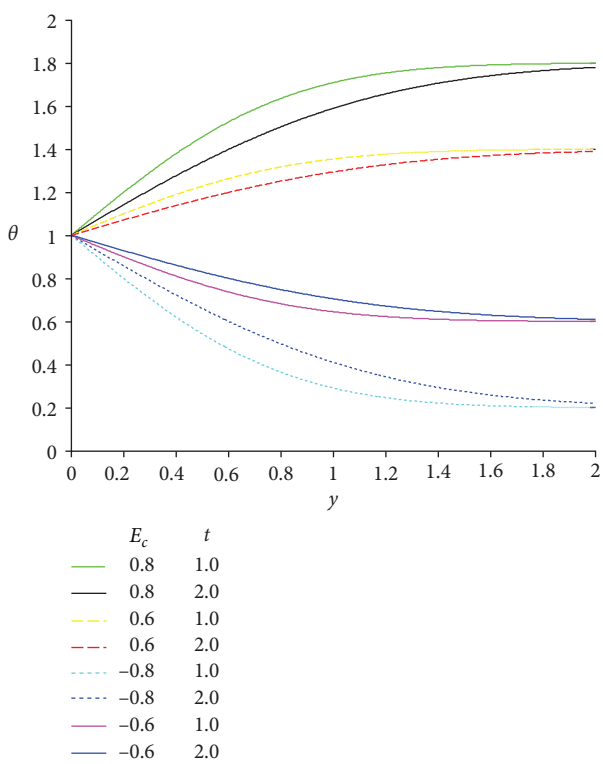


FIGURE 4: Temperature profile of the effect of $E_c$ on the electrolyte solution ($P_r = 1.0$) when $F = 2$.

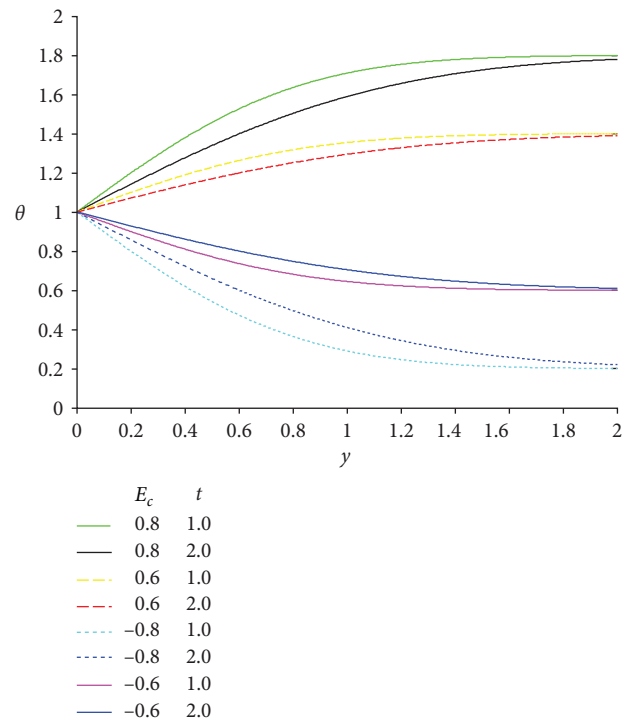


FIGURE 5: Temperature profile of the effect of $E_c$ on air ($P_r = 0.71$) when $F = 2$.

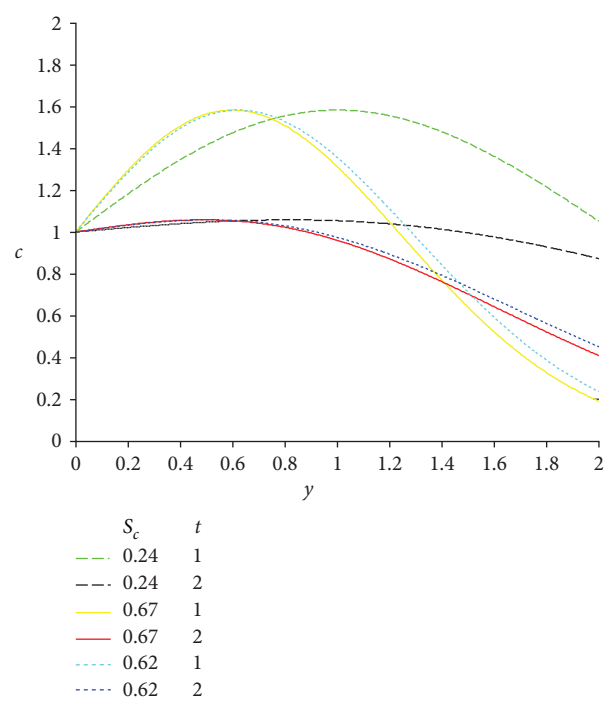


FIGURE 6: Concentration profile for electrolyte solution with $S_c = 0.67$, air with $S_c = 024$ and water with $S_c = 0.62$ when $K_c = 1$.

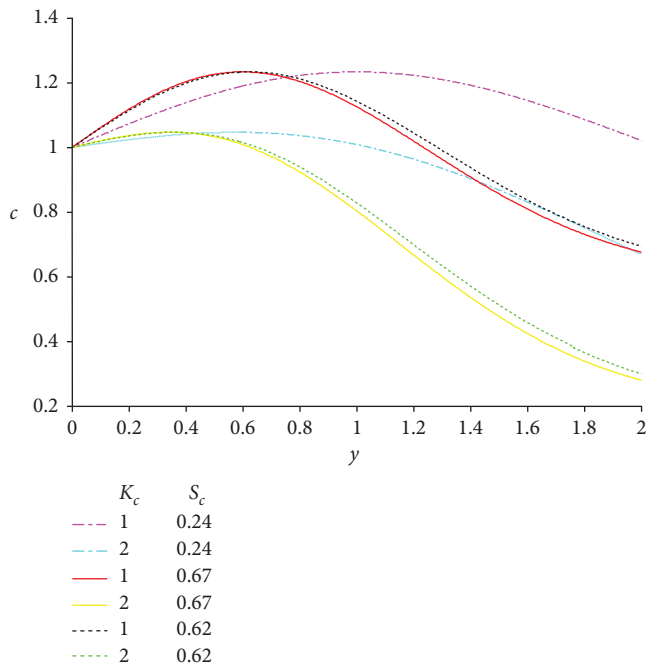


FIGURE 7: Concentration profile of the effects of rate of chemical reaction, $K_c$ on electrolyte solution with $S_c = 0.67$, air with $S_c = 0.21$, and water ($S_c = 0.62$) when $t = 0.2$.

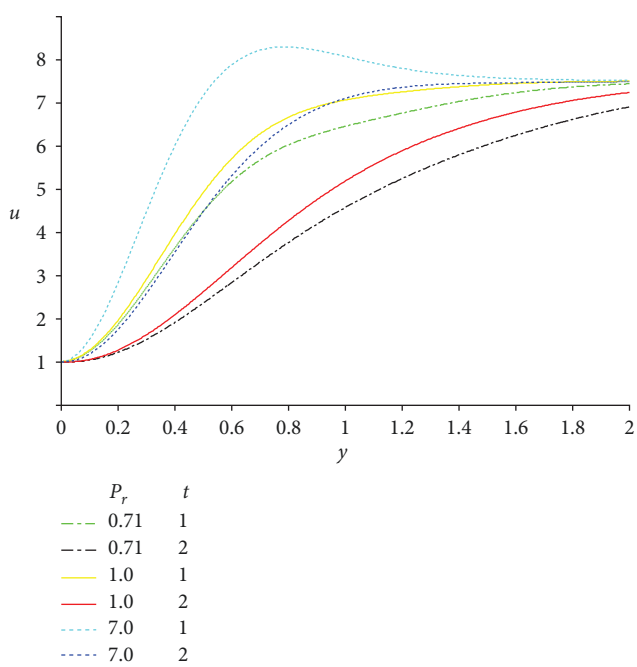


FIGURE 8: Velocity profile for air with $P_r = 0.71$, electrolyte solution with $P_r = 1.0$, and water with $P_r = 7.0$ when $G_c = 4, S_c = 2, G_r = 4, E_c = 0.9, K_c = 1, F = 4,$ and $M = 2$.

in the fluid temperature due to an increase in internal energy caused by the increased kinetic energy of the fluid. However, this effect is offset by the other factors of the fluids under study (water, electrolyte solution, and air) such as cooling due to the magnetic field and the changes in the thermodynamic properties of these fluids.

*4.1.2. Concentration Profiles.* Figure 6 illustrates the effects of the Schmidt number, $S_c$ on the concentration profile for electrolyte solution with $S_c = 0.67$, water with $S_c = 0.62$ and air with $S_c = 0.24$. It is observed that in the presence of the magnetic field, the concentration is greater for electrolyte solution with high $S_c = 0.67$ as compared to water with low

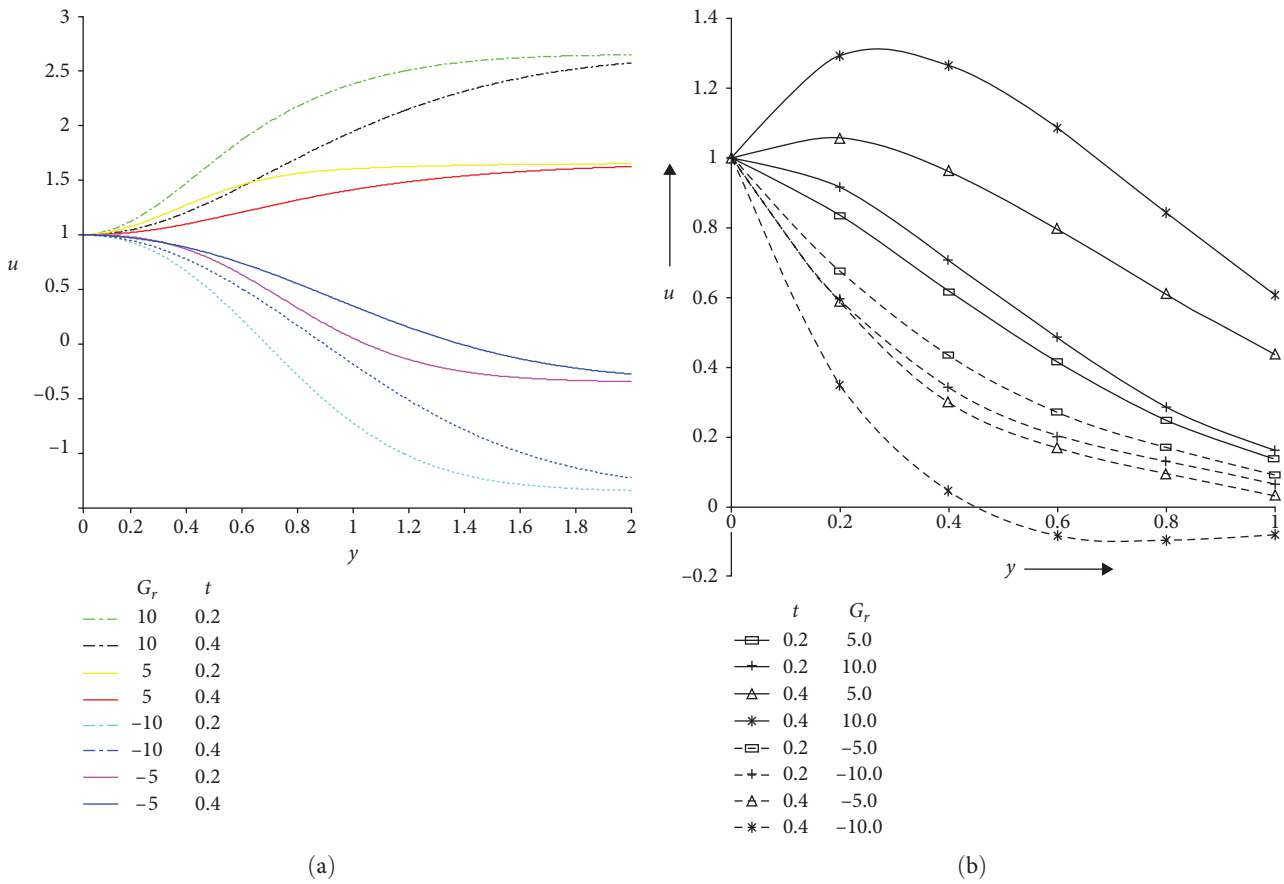


FIGURE 9: (a) Velocity profile of the effect of Grashof number $G_r$ on electrolyte solution with $P_r = 1.0$ in the present of magnetic field when $K_c = 1, G_c = 4, S_c = 2.01, E_c = 0.9, M = 3$ and $F = 3$(present study). (b) Velocity profile for electrolyte solution with $P_r = 1.0$ (in the absence of magnetic field, [27]).

$S_c = 0.62$ and air with low $S_c = 0.24$. As time elapses, the concentration diminishes faster for electrolyte solution with $S_c = 0.67$ as compared to air with $S_c = 0.24$ and water with $S_c = 0.62$, i.e., in a magnetized fluid, the presence of a magnetic field significantly affects the Schmidt number. Thus, magnetic field alters the diffusivity of both momentum and mass in the fluid. The magnetic field increased the momentum diffusivity by inducing turbulence and enhancing mixing, while decreased the mass diffusivity by suppressing the motion of ion or molecules. Due to this, the Schmidt number in magnetized fluids is significantly different from that in nonmagnetized fluids. Electrolyte solution with high-Schmidt number has applications in various fields including biology, chemistry, and engineering. i.e., in biotechnology, high-Schmidt number electrolyte solution can be used in the separation and purification of proteins, which can be achieved through electrophoresis. High-Schmidt number electrolyte solution can be also be used in the field of membrane technology. Membranes are used in the applications such as water treatment, desalination, and gas separation. The transport of ions and other species through the membrane is governed by their diffusion properties and the use of electrolyte solutions with high-Schmidt number can improve the selectivity and efficiency of the process. Also, in electrochemical processes, electrolyte solution with high-Schmidt number is useful for application in electroplating, where the uniform deposition of metal on a substrate is essential.

The effects of rate of chemical reaction $K_c$ on air with $S_c = 0.24$, electrolyte solution with $S_c = 0.67$, and water with $S_c = 0.62$ are considered in Figure 7. Similarly, concentration is greater for electrolyte solution with high $S_c = 0.67$ as compared to water with low $S_c = 0.62$ and air with low $S_c = 0.24$. As time elapses, concentration decreases faster for electrolyte solution with $S_c = 0.67$ as compared to air with $S_c = 0.24$ and water with $S_c = 0.62$.

*4.1.3. Velocity Profiles.* Figure 8 shows velocity profile for electrolyte solution with $P_r = 1.0$, water with $P_r = 7.0$, and air with $P_r = 0.71$. Increase in velocity is high for water with high Prandtl number, $P_r = 7.0$ as compared to electrolyte solution with low $P_r = 1.0$ and air with low $P_r = 0.71$ due to the effects of the magnetic field. A higher Prandtl number means that the fluid has a greater ability to conduct heat relative to its ability to transport momentum hence the velocity is high with water with high $P_r = 7.0$ as compared to the other two fluids. It is also observed that due to interplay between the magnetic field, thermal conduction, and fluid viscosity, higher Prandtl number led to an increase in fluid velocity. The velocity however, decreases for all the three fluids as time goes on.

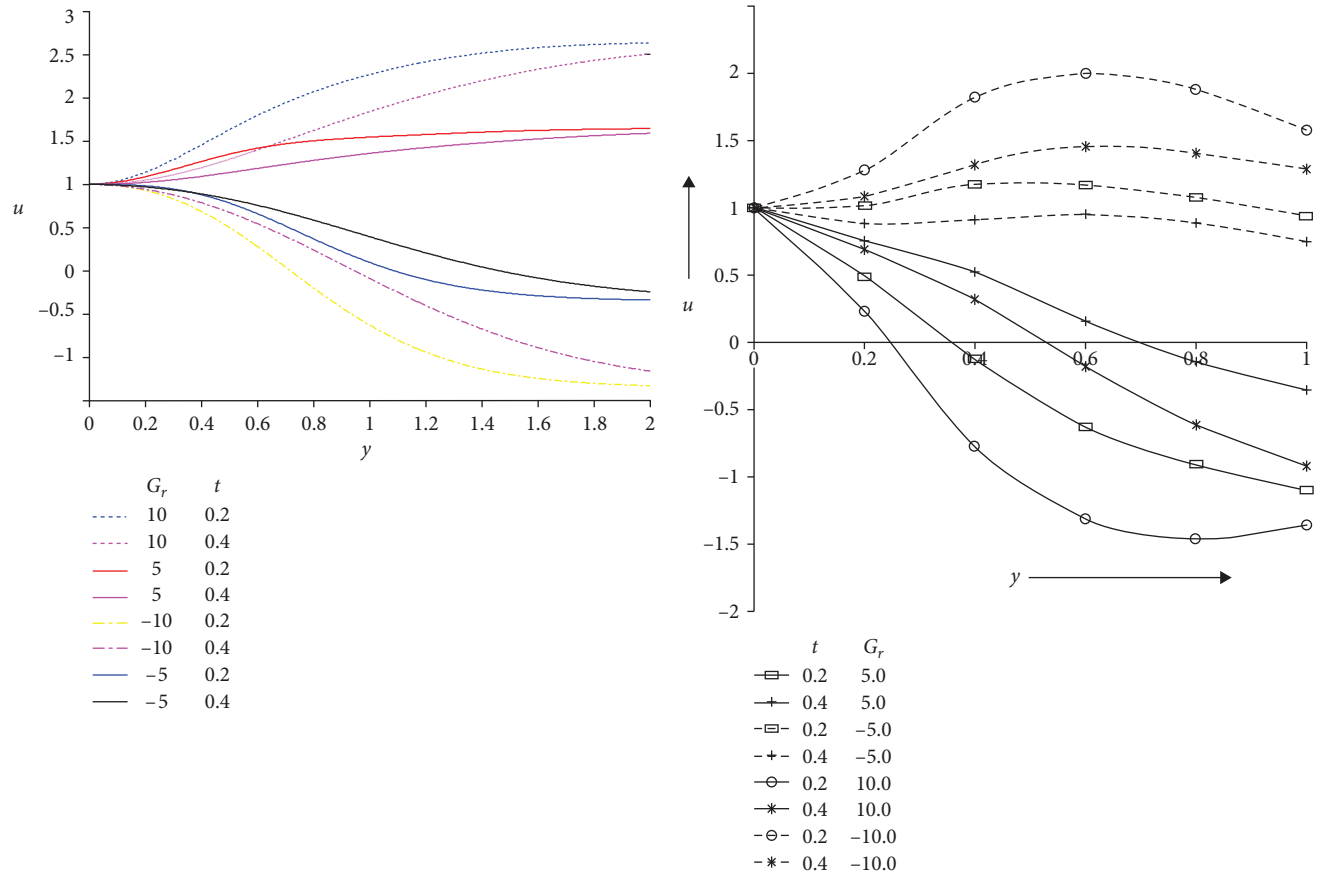


(a) (b)

FIGURE 10: (a) Velocity profile of the effect of $G_r$ on air with $P_r = 0.71$ in the present of magnetic field when $K_c = 1$, $G_c = 4$, $S_c = 2.01$, $E_c = 0.9$, $M = 3$ and $F = 3$ (present study). (b) Velocity profile for air with $P_r = 0.71$ (in the absence of magnetic field, [27]).

In Figures 9(a), 10(a), and 11(a), the effects of Grashof number $G_r$ on the velocity profile for electrolyte solution with $P_r = 1.0$, air with $P_r = 0.71$ and water with $P_r = 7.0$ are measured. Although, rise in Grashof number raised the velocity of a fluid (Figures 9(b), 10(b), and 11(b), [27]), however, with the magnetic field presence, the reverse process is observed. It is noticed that as time elapsed, the fluid velocity diminished for positive $G_r$ values but rise for negative $G_r$ values. This is so because, the presence of the magnetic field suppressed the fluid motion that is driven by buoyancy force.

The effects of $G_c$ on the velocity profile for electrolyte solution with $P_r = 1.0$, air with $P_r = 0.71$, and water with $P_r = 7.0$ are shown in Figures 12–14, respectively. Again, it is seen that the velocity diminished with time due to the magnetic field effects.

The effects of $M$ on the velocity profile for electrolyte solution with $P_r = 1.0$, air with $P_r = 0.71$, and water with $P_r = 7.0$ is illustrated in Figure 15. It is noted that the velocity rise for all the three fluids as $M$ increased. However, the increase in velocity of water with high $P_r = 7.0$ is greater as compared to the electrolyte solution with low $P_r = 1.0$ and air with $P_r = 0.71$ due to the presence of the magnetic field.

Figure 16 shows Eckert number effects on the velocity profile for water with $P_r = 7.0$, electrolyte solution with $P_r = 1.0$, and air with $P_r = 0.71$. The velocity rise with increase in Eckert number for all the fluids. Again, the velocity is greater for water with high $P_r = 7.0$ than air with low $P_r = 0.71$ and electrolyte solution with $P_r = 1.0$.

In Figure 17, the effects of $K_c$ on the velocity profile for water with $P_r = 7.0$, electrolyte solution with $P_r = 1.0$ and air with $P_r = 0.71$ is determined. It is realized that the velocities of the fluids decayed with increment in $K_c$ due to the chemically reactive magnetic field which influenced the flow field. It is observed that the chemical reaction in porous medium can alter the properties of a fluid, such as viscosity, density, and thermal conductivity, which can affect the fluid velocity. In this study, it is noticed that the chemical reaction produced a species that increased the viscosity of the three fluids hence the fluids velocities decreased. Also, the presence of the magnetic field affects fluid velocity in a porous medium. A Lorentz force arises from the interaction between the magnetic field and the charged particles in the fluid which impede the fluid motion.

*4.2. Numerical Results.* Tables 1–3 illustrates the behavior of Nusselt number, $-\theta'(0)$, Sherwood number, $-\varnothing'(0)$, and skin friction coefficient, $-u'(0)$ for various values of $t$, $M$, $E_c$, $P_r$, $S_c$, $F$, $G_c$, and $G_c$. From Table 1, Nusselt number, $-\theta'(0)$ increases with increasing values of $P_r$ and $E_c$. From Table 2, Sherwood number, $-\varnothing'(0)$ increases with increasing values

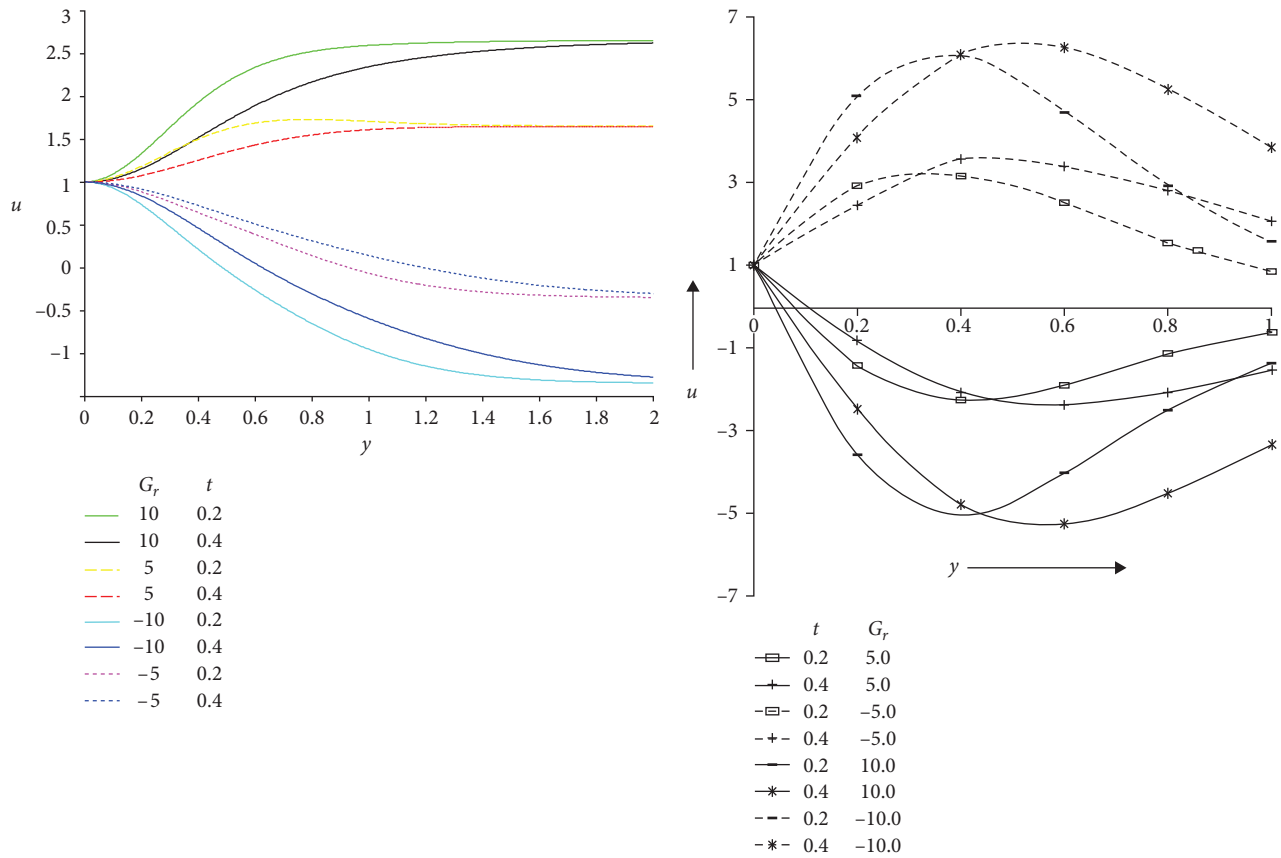


(a) (b)

FIGURE 11: (a) Velocity profile of the effect of $G_r$ on water with $P_r = 7.0$ in the present of magnetic field when $K_c = 1, G_c = 4, S_c = 2.01, E_c = 0.9, M = 3,$ and $F = 3$ (present study) (b) Velocity profile for water with $P_r = 7.0$ (in the absence of magnetic field, [27]).

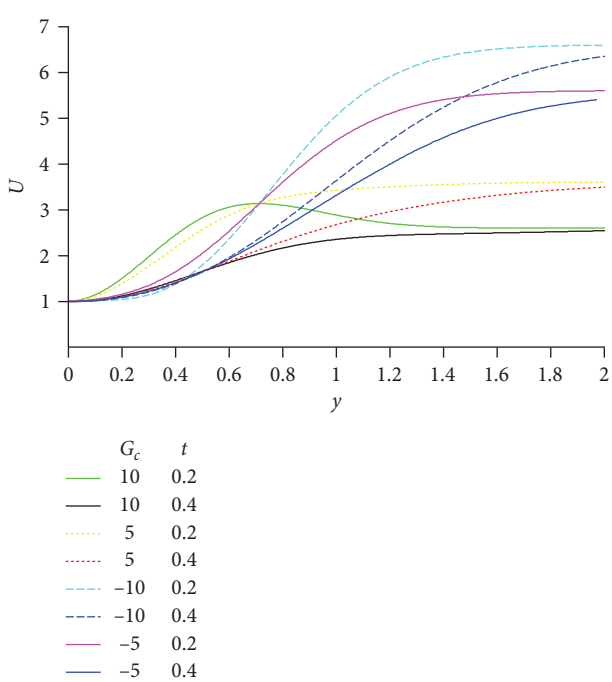


FIGURE 12: Velocity profile of the effect of $G_c$ on electrolyte solution with $P_r = 1.0$ when $K_c = 2, G_r = 4, S_c = 2.01, E_c = 0.9, M = 3,$ and $F = 3$.

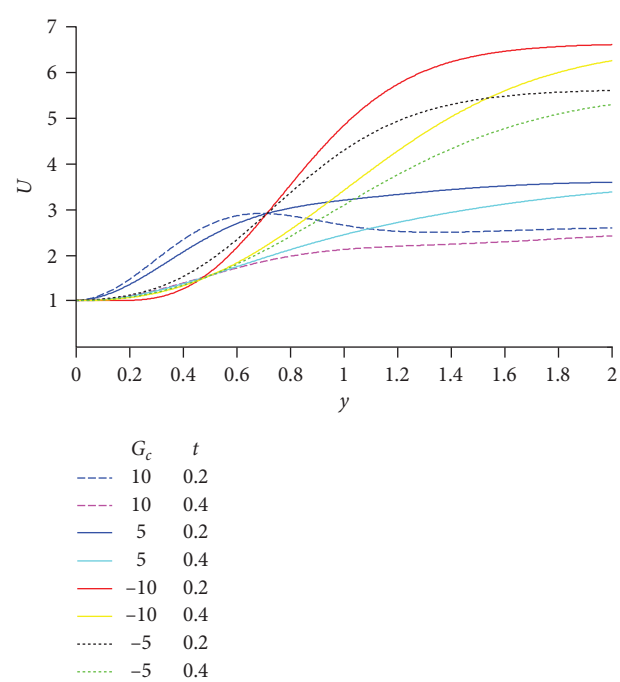


FIGURE 13: Velocity profile of the effect of $G_c$ on air with $P_r = 0.71$ when $K_c = 2, G_r = 4, S_c = 2.01, E_c = 0.9, M = 3,$ and $F = 3$.

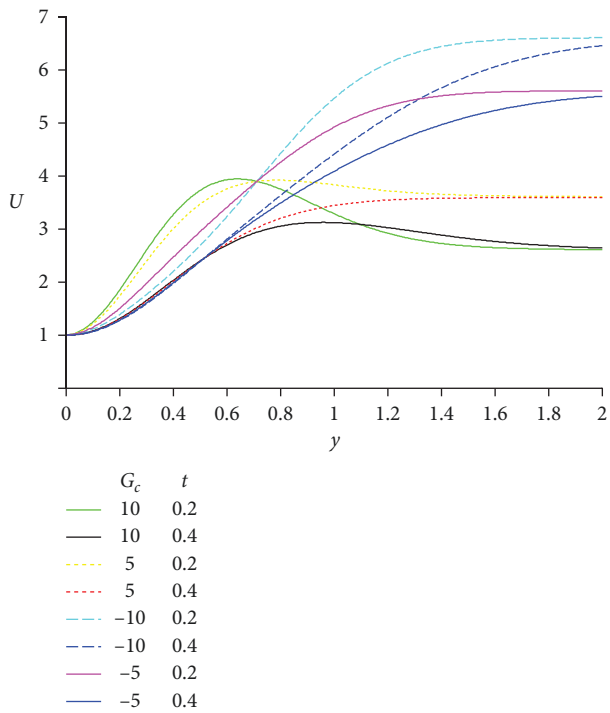


FIGURE 14: Velocity profile of the effect of $G_c$ on water with $P_r = 7.0$ when $K_c = 1, G_r = 4, S_c = 2.01, E_c = 0.9, M = 3,$ and $F = 3$.

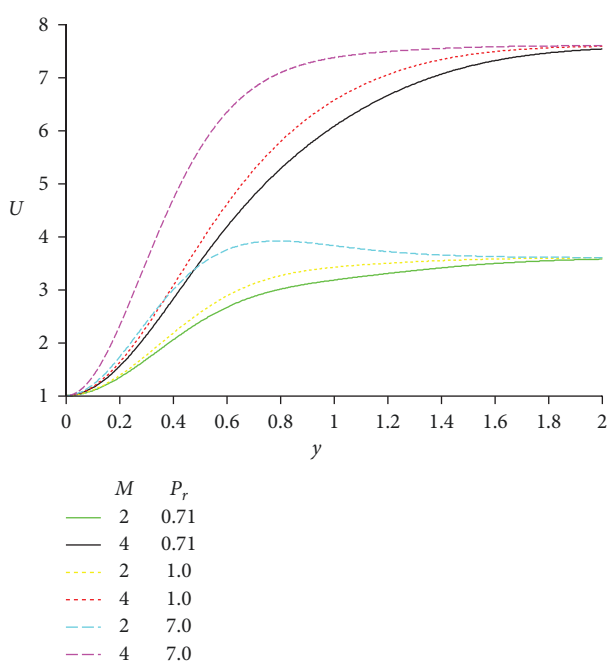


FIGURE 15: Velocity profile of the effect of $M$ on electrolyte solution with $P_r$ 1.0, air with $P_r = 0.71$, and water with $P_r = 7.0$ when $t = 2$, $K_c = 1, G_c = 4, S_c = 2.01, E_c = 0.9, G_r = 3,$ and $F = 3$.

of $E_c$ and $S_c$. From Table 3, it is noted that the skin friction coefficient, $-u'(0)$ decreases for increasing values of $t$, $M$, $E_c, G_r, G_c$ but increases for increasing values of $S_c$ and $P_r$. It is noted that, in the presence of chemically reactive magnetic porous medium, the controlling parameters such as $t, M,$

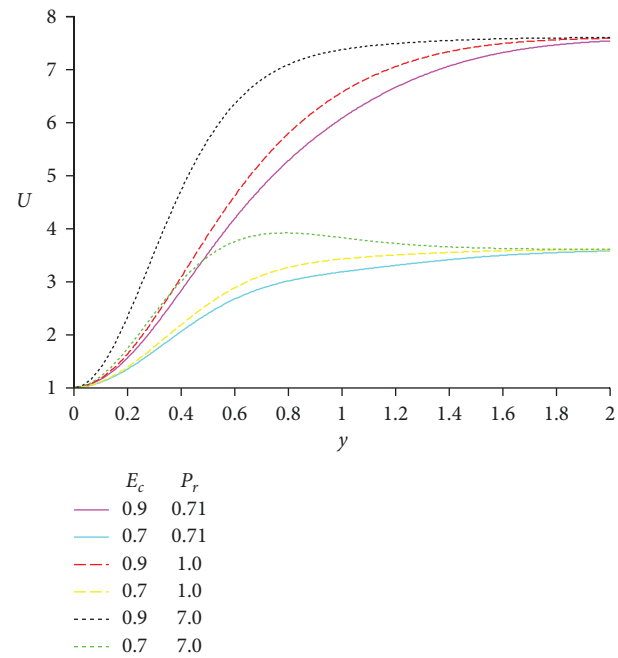


FIGURE 16: Velocity profile of the effect of $E_c$ on water with $P_r = 7.0$, electrolyte solution with $P_r = 1.0$, and air with $P_r = 0.71$ when $t = 2$, $G_c = 4, K_c = 1, S_c = 2.01, M = 3, G_r = 4,$ and $F = 3$.

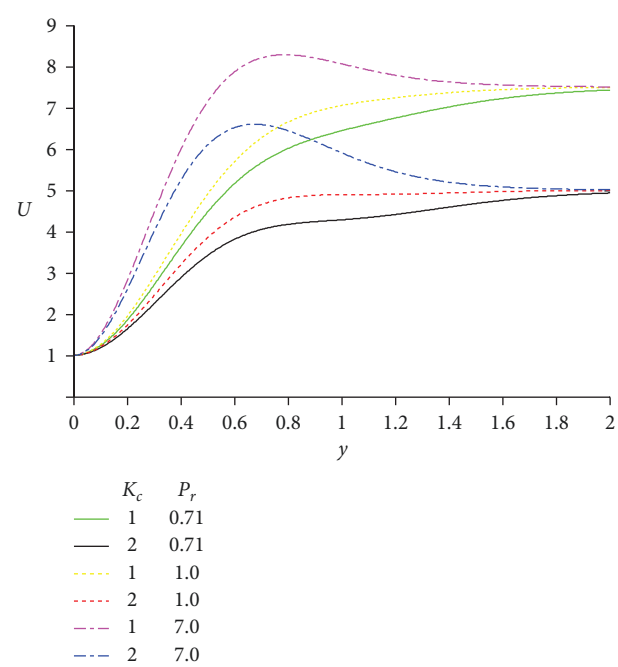


FIGURE 17: Velocity profile of the effects of $K_c$ on air ($P_r = 0.71$), electrolyte solution ($P_r = 1.0$), and water ($P_r = 7.0$) when $t = 2, G_c = 4$, $G_c = 4, E_c = 0.9, S_c = 2.01, M = 2, G_c = 4$ and $F = 2$.

$E_c$, $G_r$, and $G_c$ can be used to reduce skin friction and are relevant in practice since reduced skin friction improves efficiency of a system. In Tables 4 and 5, results of present study are compared with the previously published results of Ahmed et al. [18] and Krishna et al. [26] which showed consistency.

Table 1: The local Nusselt number, $-\theta'(0)$ at the wall, for various values of $\boldsymbol{E_c}$ and $\boldsymbol{P_r}$.

| $P_r$ | $E_c$ | $-\theta'(\mathbf{0})$ |
|---|---|---|
| **0.2** | 0.9 | 0.3800 |
| **0.4** | 0.9 | 0.7600 |
| **0.6** | 0.9 | 1.1400 |
| 0.7 | **0.2** | 0.8400 |
| 0.7 | **0.4** | 0.9800 |
| 0.7 | **0.6** | 1.1200 |

Bold values signify the increasing values of Prandtl number ($\boldsymbol{P_r}$) and Eckert number ($\boldsymbol{E_c}$).

Table 2: Sherwood number, $-\emptyset'(0)$ at the wall, for various values of $\boldsymbol{E_c}$ and $\boldsymbol{S_c}$.

| $E_c$ | $S_c$ | $-\emptyset'(\mathbf{0})$ |
|---|---|---|
| **0.2** | 0.3 | 0.6810 |
| **0.4** | 0.3 | 0.7611 |
| **0.6** | 0.3 | 0.8421 |
| 0.9 | **0.2** | 0.6199 |
| 0.9 | **0.4** | 1.3371 |
| 0.9 | **0.6** | 2.1839 |

Bold values signify the increasing values of Eckert number ($\boldsymbol{E_c}$) and Schmidt number ($\boldsymbol{S_c}$).

Table 3: The skin friction coefficient, $-u'(0)$ at the wall, for various values of $\boldsymbol{t}$, $\boldsymbol{M}$, $\boldsymbol{G_r}$, $\boldsymbol{S_c}$, $\boldsymbol{G_c}$, $\boldsymbol{P_r}$, and $\boldsymbol{E_c}$.

| $t$ | $M$ | $E_c$ | $S_c$ | $P_r$ | $G_r$ | $G_c$ | $-\boldsymbol{u}'(\mathbf{0})$ |
|---|---|---|---|---|---|---|---|
| **0.3** | 1.0 | 0.9 | 1.0 | 1.0 | 1.0 | 1.0 | 1.0353 |
| **0.5** | 1.0 | 0.9 | 1.0 | 1.0 | 1.0 | 1.0 | 0.7428 |
| **0.7** | 1.0 | 0.9 | 1.0 | 1.0 | 1.0 | 1.0 | 0.5922 |
| 0.3 | **3.0** | 0.9 | 1.0 | 1.0 | 1.0 | 1.0 | 1.6784 |
| 0.3 | **5.0** | 0.9 | 1.0 | 1.0 | 1.0 | 1.0 | 1.2372 |
| 0.3 | **7.0** | 0.9 | 1.0 | 1.0 | 1.0 | 1.0 | 0.9216 |
| 0.3 | 1.0 | **0.4** | 1.0 | 1.0 | 1.0 | 1.0 | 1.8061 |
| 0.3 | 1.0 | **0.6** | 1.0 | 1.0 | 1.0 | 1.0 | 1.4116 |
| 0.3 | 1.0 | **0.8** | 1.0 | 1.0 | 1.0 | 1.0 | 0.9643 |
| 0.3 | 1.0 | 0.9 | **4.0** | 1.0 | 1.0 | 1.0 | 0.7312 |
| 0.3 | 1.0 | 0.9 | **7.0** | 1.0 | 1.0 | 1.0 | 1.8614 |
| 0.3 | 1.0 | 0.9 | **9.0** | 1.0 | 1.0 | 1.0 | 1.9813 |
| 0.3 | 1.0 | 0.9 | 1.0 | **3.0** | 1.0 | 1.0 | 0.9821 |
| 0.3 | 1.0 | 0.9 | 1.0 | **6.0** | 1.0 | 1.0 | 1.0463 |
| 0.3 | 1.0 | 0.9 | 1.0 | **10.0** | 1.0 | 1.0 | 1.4211 |
| 0.3 | 1.0 | 0.9 | 1.0 | 1.0 | **5.0** | 1.0 | 1.9533 |
| 0.3 | 1.0 | 0.9 | 1.0 | 1.0 | **10.0** | 1.0 | 1.7312 |
| 0.3 | 1.0 | 0.9 | 1.0 | 1.0 | **15.0** | 1.0 | 1.2452 |
| 0.3 | 1.0 | 0.9 | 1.0 | 1.0 | 1.0 | **5.0** | 1.9321 |
| 0.3 | 1.0 | 0.9 | 1.0 | 1.0 | 1.0 | **10.0** | 1.7110 |
| 0.3 | 1.0 | 0.9 | 1.0 | 1.0 | 1.0 | **15.0** | 1.2101 |

Bold values signify the increasing values of physical parameters $\boldsymbol{t}$, $\boldsymbol{M}$, $\boldsymbol{E_c}$, $\boldsymbol{S_c}$, $\boldsymbol{P_r}$, $\boldsymbol{G_r}$ and $\boldsymbol{G_c}$.

Table 4: Comparism of velocity results, $S_c = 0.22$, $M = 0.5$, $P_r = 0.71$, $k_c = 0.5$, $F = 1$, $t = 1$, $G_r = 5$, $F = 0.5$, $E_c = 0.3$, $\omega = 0$, and $y = 2$.

| $G_c$ | Ahmed et al. [18] (Crank–Nicolson method) | Krishna et al. [26] (Laplace transform techniques) | Sulemana et al. [17] (AAM) | Present study (AAM) |
|---|---|---|---|---|
| 5 | 0.384885 | 0.384775 | 0.384863 | 0.384871 |
| 10 | 0.548079 | 0.547087 | 0.548157 | 0.548166 |
| 12 | 0.632847 | 0.632256 | 0.632646 | 0.632637 |

Table 5: Comparism of concentration results, $E_c = 0.3$, $t = 1$, $k_c = 0.5$, and $y = 2$.

| $S_c$ | Ahmed et al. [18] (Crank–Nicolson method) | Krisna et al. [26] (Laplace Transform Techniques) | Sulemana et al. [17] (AAM) | Present study (AAM) |
|---|---|---|---|---|
| 0.3 | 0.228051 | 0.228774 | 0.227642 | 0.227651 |
| 0.6 | 0.167541 | 0.164551 | 0.167632 | 0.167643 |
| 0.78 | 0.084308 | 0.081447 | 0.083421 | 0.083434 |

## 5. Conclusion

In this study, we have investigated unsteady MHD hydrodynamic convective heat and mass transfer subject to Newtonian heating in a porous medium. Using dimensionless variables, the nonlinear partial differential equations have been derived and transformed into dimensionless differential equations which are solved by means of approximate analytical method and results illustrated both graphically and numerically. The findings drawn from the study are:

(1) The thermal boundary layer thickness is greater for water with high $P_r = 7.0$ when compared to air with low $P_r = 0.71$ and electrolyte solution with low $P_r = 1.0$ in the presence of the magnetic field but diminishes with time. Practically, water with a high-Prandtl number can be used as a heat transfer fluid in heating and cooling systems. It can effectively absorb and release heat, which makes it useful in the applications such as geothermal heat pumps and solar thermal collectors.

(2) High concentration is observed for electrolyte solution with high $S_c = 0.67$ when compared with water with low $S_c = 0.62$ and air with low $S_c = 0.24$ but as time elapsed the electrolyte solution diminished faster as compared with water and air. Electrolyte solution with high-Schmidt number has practical applications in the electrochemistry, biotechnology, and membrane technology.

(3) The velocity increased with increased in Eckert number ($E_c$), magnetic parameter ($M$) but decreased with increas in rate of chemical reaction ($K_c$) for all the thre fluids.

(4) Though, the effect of an increase in Grashof number is to raise the velocity values. Due to the presence of the magnetic field, it is observed that as time goes on, the velocity decreases for positive values of $G_r$ but increases for negative values of $G_r$.

(5) The rate of cooling associated with air, water, or electrolyte impacts differently on the product being cooled.

## Nomenclature

$u^*, v^*$: x and y Components of velocity, respectively ($\mathrm{ms}^{-1}$)
$U_0$: Velocity of the plate ($\mathrm{ms}^{-1}$)
$y^*$: Coordinate axis normal to the plate ($m$)
$t^*$: Time ($s$)
$\nu$: Kinematic viscosity ($m^2 s^{-1}$)
$\beta_T$: Thermal expansion coefficient ($K^{-1}$)
$\beta_C$: Concentration expansion coefficient ($K^{-1}$)
$\rho$: Fluid density ($\mathrm{kgm}^{-3}$)
$T^*$: Fluid temperature near the plate ($K$)
$T_w^*$: Fluid temperature at the plate surface ($K$)
$T_\infty^*$: Temperature of the free stream ($K$)
$C^*$: Concentration in the fluid ($\mathrm{Kmolm}^{-3}$)
$C_\infty^*$: Concentration far away from the plate ($\mathrm{Kmolm}^{-3}$)
$C_w^*$: Concentration at the plate surface ($\mathrm{Kmolm}^{-3}$)
$a$: Acceleration parameter (–)
D: Chemical molecular diffusivity ($m^{-2}s^{-1}$)
$\propto$: Thermal diffusivity ($m^2K^{-1}$)
$C_p$: Specific heat at constant pressure ($\mathrm{Jkg}^{-1}K^{-1}$)
$K_c^*$: Rate of chemical reaction (–)
$k^*$: Permeability coefficient of the porous medium ($m^2$)
$q_r$: Radiation heat flux (–)
$Q$: Heat source parameter (–)
$y$: Dimensionless coordinate axis normal to the plate surface (–)
$u$: Dimensionless velocity in $x$ direction (–)
$v$: Dimensionless velocity in $y$ direction (–)
$\theta$: Dimensionless temperature (–)
$t$: Dimensionless time (–)
$k$: Dimensionless permeability of the porous medium (–)
$F$: Radiation parameter (–)
$M$: Magnetic parameter (–)
$H$: Heat absorption parameter (–)
$A$: Constant (–)
$B_0$: Uniform external magnetic field (Telsa)
$\mu$: Dynamic viscosity ($\mathrm{kgm}^{-1}s^{-1}$)
$S_0$: Soret number (–)
$S_c$: Schmidt number (–)
$P_r$: Prandtl number (–)
$G_r$: Thermal Grashof number (–)
$G_c$: Mass Grashof number (–)
$\sigma$: Electrical conductivity ($\mathrm{sm}^{-1}$)
$\varnothing$: Dimensionless concentration in the fluid (–)
$g$: Acceleration due to gravity ($\mathrm{ms}^{-2}$)
$K$: Thermal conductivity of the fluid ($\mathrm{Wm}^{-1}K^{-1}$)
$K_C$: Dimensionless rate of chemical reaction (–)
$E_c$: Eckert number (–)
$a^*$: Rosseland mean absorption coefficient (–-)
$\sigma^*$: Stefan–Boltzman constant (–).

## Data Availability

Numerical data used to support the findings of this study are included within the article.

## Conflicts of Interest

The authors declare that there is no conflict of interest regarding the publication of this paper.

## Acknowledgments

This research work is built from my (Dr. Musah Sulemana) thesis under the supervision of Prof. Yakubu Ibrahim Seini but solved with new enhanced technique "Approximate Analytic Method" under the advice of Prof. Oluwole Daniel Makinde.

## References

[1] R. Siegel, "Transient free convection from a vertical flat plate," *Journal of Fluids Engineering*, vol. 80, no. 2, pp. 347–357, 1958.

[2] O. G. Martynenko, A. A. Berezovsky, and Y. A. Sokovishin, "Laminar free convection from a vertical plate," *International Journal of Heat and Mass Transfer*, vol. 27, no. 6, pp. 869–881, 1984.

[3] U. N. Das, R. K. Deka, and V. M. Soundalgeker, "Radiation effects on flow past an impulsively started infinite vertical plate with constant mass flux-An exact solution," *Heat and Mass*, vol. 3, pp. 163–167, 1996.

[4] S. Das, C. Mandal, and R. N. Jana, "Radiation effects on unsteady free convection flow past a vertical plate with Newtonian heating," *International Journal of Computer Applications*, vol. 41, no. 13, pp. 36–41, 2012.

[5] S. Manjunatha, B. J. Gireesha, and C. S. Bagewadi, "Effect of thermal radiation on boundary layer flow and heat transfer of dusty fluid over an unsteady stretching sheet," *International Journal of Engineering, Science and Technology*, vol. 4, no. 4, pp. 36–48, 2012.

[6] S. Das, R. N. Jana, and A. J. Chamkha, "Unsteady free convection flow past a vertical plate with heat and mass fluxes in the presence of thermal radiation," *Journal of Applied Fluid Mechanics*, vol. 8, no. 4, pp. 845–854, 2015.

[7] S. Das and R. N. Jana, "Natural convective magneto-nanofluid flow and radiative heat transfer past a moving vertical plate," *Alexandria Engineering Journal*, vol. 54, no. 1, pp. 55–64, 2015.

[8] M. K. A. Mohamed, M. Z. Salleh, N. A. Z. M. Noar, and A. Ishak, "Effect of thermal radiation on laminar boundary layer flow over a permeable flat plate with Newtonian heating," *Journal of Physics: Conference Series*, vol. 890, Article ID 012007, 2017.

[9] K. J. Basant and S. Gabriel, "Thermal radiation effect on boundary layer over flow a flat plate having convective surface boundary condition," *SN Applied Sciences*, vol. 2, Article ID 381, 2020.

[10] M. Hussain, J. Cui, U. Farooq, M. E. A. Rabie, and T. Muhammad, "Nonsimilar modeling and numerical simulations of electromagnetic radiative flow of nanofluid with entropy generation," *Mathematical Problems in Engineering*, vol. 2022, Article ID 4272566, 20 pages, 2022.

[11] K.-L. Hsiao, "Heat and mass mixed convection for MHD viscoelastic fluid past a stretching sheet with ohmic dissipation," *Communications in Nonlinear Science and Numerical Simulation*, vol. 15, no. 7, pp. 1803–1812, 2010.

[12] K.-L. Hsiao, "MHD stagnation point viscoelastic fluid flow and heat transfer on a thermal forming stretching sheet with viscous dissipation," *The Canadian Journal of Chemical Engineering*, vol. 89, no. 5, pp. 1228–1235, 2011.

[13] S. Nadeem, R. U. Haq, N. S. Akbar, and Z. H. Khan, "MHD three-dimensional Casson fluid flow past a porous linearly stretching sheet," *Alexendra Engineering Journal*, vol. 52, no. 4, pp. 577–582, 2013.

[14] Y. I. Seini and O. D. Makinde, "MHD boundary layer flow due to exponential stretching surface with radiation and chemical reaction," *Mathematical Problems in Engineering*, vol. 2013, Article ID 163614, 7 pages, 2013.

[15] M. Ali, M. A. Alim, and M. S. Alam, "Heat transfer boundary layer flow past an inclined stretching sheet in presence of magnetic field," *International Journal of Advancements in Research & Technology*, vol. 3, no. 5, pp. 34–40, 2014.

[16] M. Sulemana and I. Y. Seini, "Time-dependent hydromagnetic boundary layer flow across a porous vertical surface with internal heat generation," *Defect and Diffusion Forum*, vol. 409, pp. 17–38, 2021.

[17] M. Sulemana, I. Y. Seini, and O. D. Makinde, "Hydrodynamic boundary layer flow of chemically reactive fluid over exponentially stretching vertical surface with transverse magnetic field in unsteady porous medium," *Journal of Applied Mathematics*, vol. 2022, Article ID 7568695, 11 pages, 2022.

[18] S. Ahmed, A. Batin, and A. J. Chamkha, "Numerical/Laplace transform analysis for MHD radiating heat/mass transport in a Darcian porous regime bounded by an oscillating vertical surface," *Alexandria Engineering Journal*, vol. 54, no. 1, pp. 45–54, 2015.

[19] W. Ibrahim and A. Tulu, "Magnetohydrodynamic (MHD) boundary layer flow past a wedge with heat transfer and viscous effects of nanofluid embedded in porous media," *Mathematical Problems in Engineering*, vol. 2019, Article ID 4507852, 12 pages, 2019.

[20] K. Jabeen, M. Mushta, and R. M. Akram, "Analysis of the MHD boundary layer flow over a nonlinear stretching sheet in porous medium using semianalytical approaches," *Mathematical Problems in Engineering*, vol. 2020, Article ID 3012854, 9 pages, 2022.

[21] Y. D. Reddy, F. Mebarek-Oudina, B. S. Goud, and A. I. Ismail, "Radiation, velocity and thermal slips effect toward MHD boundary layer flow through heat and mass transport of Williamson nanofluid with porous medium," *Arabian Journal for Science and Engineering*, vol. 47, no. 12, pp. 16355–16369, 2022.

[22] E. Arul Vijayalakshmi, S. S. Santra, T. Botmart et al., "Analysis of magnetohydrodynamic flow in porous medium," *AIMS Mathematics*, vol. 7, no. 8, pp. 15182–15194, 2022.

[23] M. Hussain, W. Khan, U. Farooq, and R. Razzaq, "Impact of non-similar modeling for thermal transport analysis of mixed convective flows of nanofluids over vertically permeable surface," *Journal of Nanofluids*, vol. 12, no. 4, pp. 1074–1081, 2023.

[24] Y. I. Seini, "Flow over unsteady stretching surface with chemical reaction and non-uniform heat source," *Journal of Engineering and Manufacturing Technology*, vol. 1, no. 2, pp. 24–35, 2013.

[25] M. Sulemana, I. Y. Seini, and M. I. Daabo, "Unsteady boundary layer flow past a vertical plate in the presence of transverse magnetic field and heat source embedded in a porous medium," *Journal of Mathematical and Computational Science*, vol. 7, no. 3, pp. 564–582, 2017.

[26] M. V. Krishna, M. G. Reddy, and A. J. Chamkha, "Heat and mass transfer on unsteady mhd flow through an infinite oscillating vertical porous surface," *Journal of Porous Media*, vol. 24, no. 1, pp. 81–100, 2021.

[27] R. C. Chaudhary and P. Jain, "Unsteady free convection boundary-layer flow past an impulsively started vertical surface with Newtonian heating," *Romanian Journal of Physics*, vol. 51, no. 9, pp. 911–925, 2006.

[28] M. Narahari and M. Y. Nayan, "Free convection flow past an impulsively started infinite vertical plate with Newtonian heating in the presence of thermal radiation and mass diffusion," *Turkish Journal of Engineering and Environmental Sciences*, vol. 35, pp. 187–198, 2011.

[29] A. Hussanan, M. Zuki Salleh, R. M. Tahar, and I. Khan, "Unsteady boundary layer flow and heat transfer of a Casson fluid past an oscillating vertical plate with Newtonian heating," *PLoS One*, vol. 9, no. 10, Article ID e108763, 2014.

[30] S. Sharidan, H. Abid, I. Khan, and M. Z. Salleh, "Slip effects on unsteady free convective heat and mass transfer flow with Newtonian heating, 142-143," *Thermal Science*, vol. 20, no. 6, 2014.

[31] A. Hussanan, M. Z. Salleh, I. Khan, R. M. Tahar, and Z. Ismail, "Soret effects on unsteady MHD mixed convective heat and mass transfer flow in a porous medium with Newtonian heating," *Maejo International Journal of Science and Technology*, vol. 9, no. 2, pp. 224–245, 2015.

[32] H. Konwar, B. Bendangwapang, and T. Jamir, "Mixed convection MHD boundary layer flow, heat, and mass transfer past an exponential stretching sheet in porous medium with temperature-dependent fluid properties," *Numerical Heat Transfer, Part A: Applications: An International Journal of Computation and Methodology*, vol. 83, no. 12, pp. 1346–1364, 2023.

[33] M. Sulemana, "Unsteady magnetohydrodynamics heat and mass transfer through porous media," 2019.